FULL PAPER

Foot Pressure Mapping

ADVANCED
FUNCTIONAL
MATERIALS

www.afm-journal.de

Self-Powered Insole Plantar Pressure Mapping System

Chaoran Deng, Wei Tang, Long Liu, Baodong Chen, Meicheng Li,*
and Zhong Lin Wang*

Sensitive monitoring and real-time foot pressure mapping have important applications for medical treatment/diagnostics, sports training, and even security. In this work, a facile plantar pressure mapping system with a large pressure detection range using piezoelectric nanogenerators serving as the sensor array to acquire pressure signals, and a self-designed data acquisition (DAQ) circuit board to process and wirelessly send the signals to a mobile terminal, such as a smart phone, are developed. Working with an application program developed in Android, the whole system can accurately monitor and visually display the real-time pressure distribution during walking. More importantly, by combining a hybridized triboelectric–electromagnetic nanogenerator, a self-powered, continuous, and real-time pressure distribution monitoring system is developed, which provides a feasible solution for sport/exercise biomechanics information acquisition, injury prevention, and ulceration prediction in the feet.

1. Introduction

There have been profound research works aiming at monitoring humanity physiological signals for disease prophylaxis and treatment,[1] health assessment,[2] tactile (or touch) sensing

C. Deng, Prof. W. Tang, Dr. L. Liu, Dr. B. Chen, Prof. Z. L. Wang
CAS Center for Excellence in Nanoscience
Beijing Key Laboratory of Micro-nano Energy and Sensor
Beijing Institute of Nanoenergy and Nanosystems
Chinese Academy of Sciences
Beijing 100083, P. R. China
E-mail: zhong.wang@mse.gatech.edu
C. Deng, Prof. W. Tang, Dr. L. Liu, Dr. B. Chen, Prof. Z. L. Wang
College of Nanoscience and Technology
University of Chinese Academy of Sciences
Beijing 100049, P. R. China
Prof. M. C. Li
State Key Laboratory of Alternate Electrical Power System with
Renewable Energy Sources
School of Renewable Energy
North China Electric Power University
Beijing 102206, China
E-mail: mcli@ncepu.edu.cn
Prof. Z. L. Wang
School of Materials Science and Engineering
Georgia Institute of Technology
Atlanta, GA 30332-0245, USA

The ORCID identification number(s) for the author(s) of this article can be found under https://doi.org/10.1002/adfm.201801606.

even security application by developing wearable/portable and sensitive nanogenerator-based sensors.[3] More often, sensors focusing on diagnosis or precaution could meet practical demand by discovering bioelectric signals from special point, such as blood pressure from the radial artery revealing arterial sclerosis,[4] movement of body and eyeballs telling sleep disorder,[2b,c] and motion of respiratory muscles for diagnosis of respiratory disease,[5] respectively. Meanwhile, the foot pressure distribution not only can suggest footwear design and sport biomechanics information, but also indicate possible injury and even predict ulceration in the feet of patients with type 2 diabetes.[6] Specifically, plantar pressure values from a lot of areas, including heel, lateral mid foot, metatarsal, and so on, can serve as a necessary medical indication.[6]

Intensive efforts have been devoted on pressure sensors with piezoelectric nanogenerator (PENG), triboelectric nanogenerator (TENG), or ferroelectric layer. Sensors based on piezoelectric materials like ZnO,[7] lead zirconate titanate (PZT),[8] MoS_2,[9] poly (vinylidene fluoride) (PVDF) and its similar copolymer p(vdf-TrFE) have exhibit excellent performance through converting mechanical signal into electrical output.[10] Owing to the advantage of good piezoelectric and mechanical properties, high and chemical stability, β-phase PVDF is considered as one of the most suitable materials for clinically oriented body pressure measurement.[6d]

In this paper, we developed a smart insole to monitor and display the foot pressure at real time. Instead of using multistep microstructure processes, a flexible printed circuit board (FPC) with 32 pieces of PVDF as the PENG pressure sensors (PENG-PS) is employed, which can be large quantity manufactured at low cost. To convert the raw sensor signal to digital signal, the FPC with PENG-PS attached is connected to a designed data acquisition circuit (DAQ). These converted results can be transmitted to mobile terminal, such as laptop, pad, and smart phone through Bluetooth 4.2 protocol, then the real-time pressure distribution is reconstructed. Furthermore, the DAQ can work at low active current, which could be powered by the designed nanogenerators in our previous work.[11] More importantly, through driving by a hybridized triboelectric–electromagnetic nanogenerator, a self-powered and real-time pressure mapping system is demonstrated. This work can serve as an important guidance for footwear design, sport/exercise biomechanics information acquisition, and self-powered sensor applications in the future.
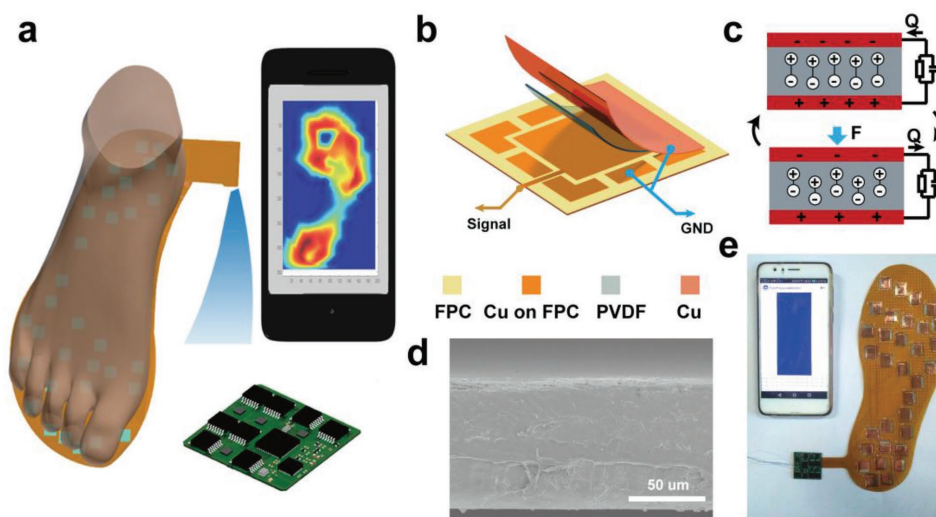
Figure 1. Schematic illustration of a plantar pressure monitoring system. a) Schematic illustration of system for foot pressure distribution monitoring. b) Structure of a sensor nodes comprising PVDF slice and FPC. c) Working principle for a single pizeo-pixel at compressive force. d) SEM image of the PVDF thin film. e) Optical photograph of whole monitoring system.

2. Result and Discussion

2.1. Fabrication and Characterization of the PENG Pressure Sensor

Figure 1a illustrates that the whole system is composed of three parts: an insole-shaped FPC broad with PENG-PS, a DAQ circuit, and an application software on smart phone. The β-phase PVDF film which used as PENG pressure sensor can be obtained by several techniques, among which the mechanical stretching of the melted-and-cooled PVDF solution, namely α-phase PVDF film, is the most accepted method in industrial production.[12] The insole-shaped FPC broad, which can be mass-produced with Kapton film as flexible plastic substrates, were printed 32 pads to fix the PVDF pieces with the same size. The layout of the FPC broad is mainly used to satisfy the requirements for both medical diagnosis and pressure mapping. As shown in Figure 1b, after clipped into small squares in the size of 10×10 mm^2, each double-sided aluminized PVDF slice with a thickness of 100 µm (the scanning electron microscope (SEM) image of the PVDF thin film is shown in Figure 1d) is fixed and connected to the signal pad on the FPC by copper powder conductive adhesive (blue pad and routing in Figure 1b). Meanwhile, the other electrode is connected to the printed layout using copper tape as a common ground plane. This structure guarantees that the foot plantar applies pressure against the ground electrodes. The working principle of PVDF as a PENG or a pressure transducer, has been detailed reported in previous work.[13] As illustrated in Figure 1c, a vertical mechanical deformation results in the generation of force-associated piezoelectric polarization charges at both the ends of the material. Because of these polarization charges, the electrostatic potential drives free electrons flowing from one electrode to the other though external load.

Before connecting to a low-power conversion circuit, the output performances of the PVDF film on FPC, including open circuit voltage (V_{OC}) and free charges were measured. Especially the measured film was encapsulated with an Epoxy glass fiber (FR4) lamination (13.5×13.5 mm^2 in size, and 0.3 mm in thickness). The packaged PENG-PS was attached onto a linear motor, then cyclic external pressure is applied and recorded by a dynamometer (HANDPI digital Push & Pull Tester, HP-1K), as shown in Figure S1 in the Supporting Information. Through applying series different magnitude but same motion period cyclic pressures, the results of V_{OC} of the PENG-PS are demonstrated in **Figure 2**a. It can be observed that the V_{OC} stays at quite low level when there is no pressure and rises to a higher value after applying the external force. As shown in Figure 2b, there is a direct linear relationship between the measured V_{OC} and the external pressure, so that the magnitude of external pressure can be measured by V_{OC} in a fairly large range with single sensitivity of 0.008 V kPa^{-1}. The sensitivity is defined by

$$S = \frac{\Delta V}{\Delta P} \tag{1}$$

Similarly, the Figure 2c presents the free charge movements of PENG-PS during squeeze–release cyclic motion at the same speed but varying pressures. The output stays low when there is no contact pressure, then rises with the increase of external pressure, and finally, decreases to initial state as withdrawing the external force. A direct linear relationship between free charges and contact pressure is shown in Figure 2d. It indicates that the free charges can reflect the pressure applied on the sample with the sensitivity of 23.4 pC N^{-1}, which is close to the value of PVDF piezoelectric charge constant $21 \pm 1\%$ pC N^{-1} given by vendors. The sensitivity is defined by

$$S = \frac{\Delta Q}{A \cdot \Delta P} \tag{2}$$

where the A is the area of the PVDF film.

2.2. Charge Amplifier

To measure and utilize the charge–pressure response of the PVDF film sensor, the Charge Amplifier (CAmp) circuit is
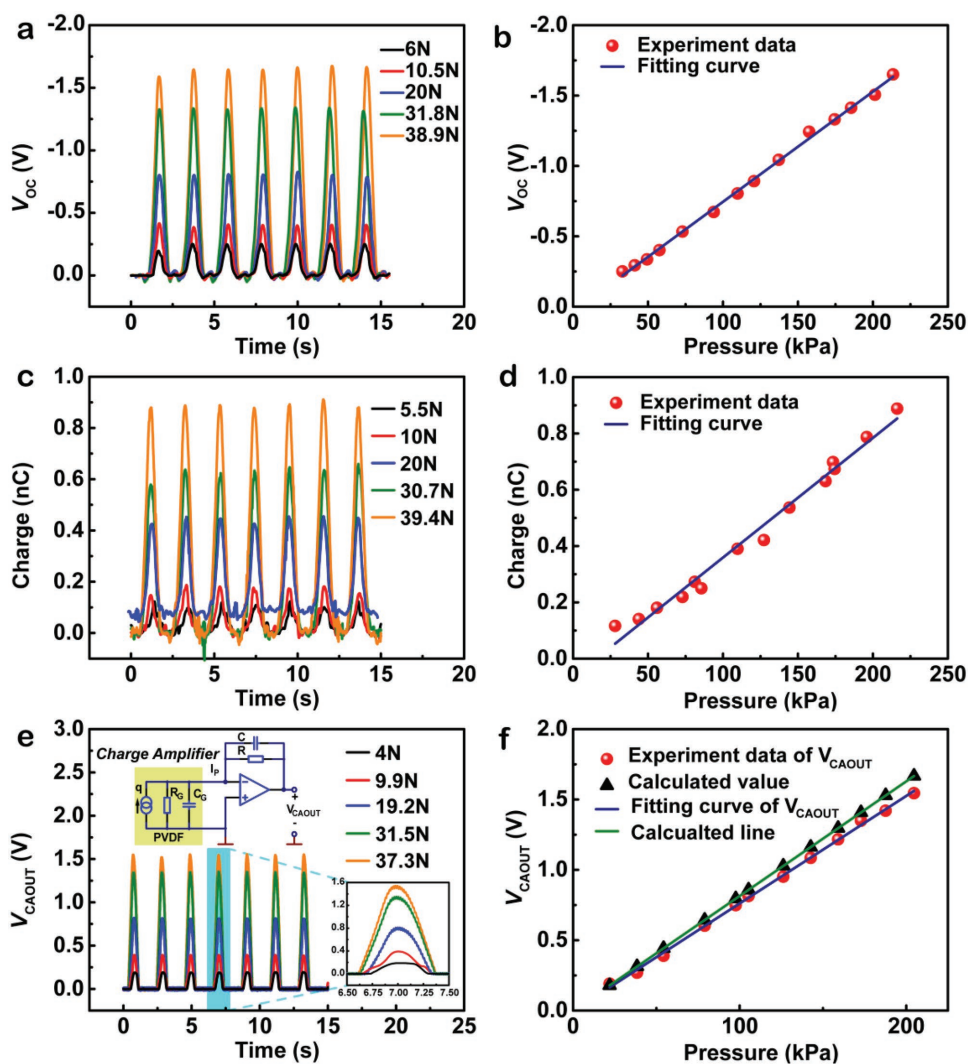
Figure 2. Electromechanical response of the PENG-PS. a) Real-time measurement of the relative change of open circuit voltage (V_{OC}) with cyclic and variable pressures applied on the PENG-PS. b) The summarized relationship and linear fitting between the relative variations (V_{OC}) and the pressure applied on PENG-PS. c) The real-time measurement of the free charge with cyclic and variable pressures applied on the sensor. d) The measured free charge changes as a function of the applied pressure. e) The real-time measurement of the output voltage of CAmp (V_{CAOUT}) with cyclic and variable pressures applied on the PENG-PS. The upper inset part is the equivalent circuit schematic diagram of the Camp and PVDF. f) The summarized relationship and linear fitting between the calculated result, measured V_{CAOUT} and the applied pressure.

employed,[10f] which is used to transform charges' amount to voltage signal V_{CAOUT}. The V_{CAOUT} is approximately proportional to the charges, which can be described by the following equation

$$V_{CAOUT} = \frac{Q}{C} \qquad (3)$$

$$Q = \sum_i d_{3i} P_i \qquad (4)$$

where the C is the capacitor composing negative feedback loop in the CAmp, Q is the external free charge produced by PVDF film, which is a function of the external force P_i. According to the Equation (3), Q can be obtained by the measured V_{CAOUT}. Therefore, the applied force P_i can be calculated out. Figure 2e shows the measured V_{CAOUT} under

different compressive force. As the force increased from 4 to 37.3 N, the V_{CAOUT} increased from 0.2 to 1.6 V. The upper inset shows a schematic illustration of the CAmp. In Figure 2f, the measured V_{CAOUT} and calculated results from Equations (3) and (4) are compared. It can be noticed that the measured V_{CAOUT} sensitivity is 0.00764 V kPa^{-1}, which is close to the calculated sensitivity of 0.00814 V kPa^{-1} in a wide range up to 200 kPa. Where the measured V_{CAOUT} sensitivity is defined by

$$S = \frac{\Delta V_{CAOUT}}{\Delta P} \qquad (5)$$

As shown in Figure S2a in the Supporting Information, there are few distortions and noise, further demonstrating the correction of the Equation (3) in the CAmp.
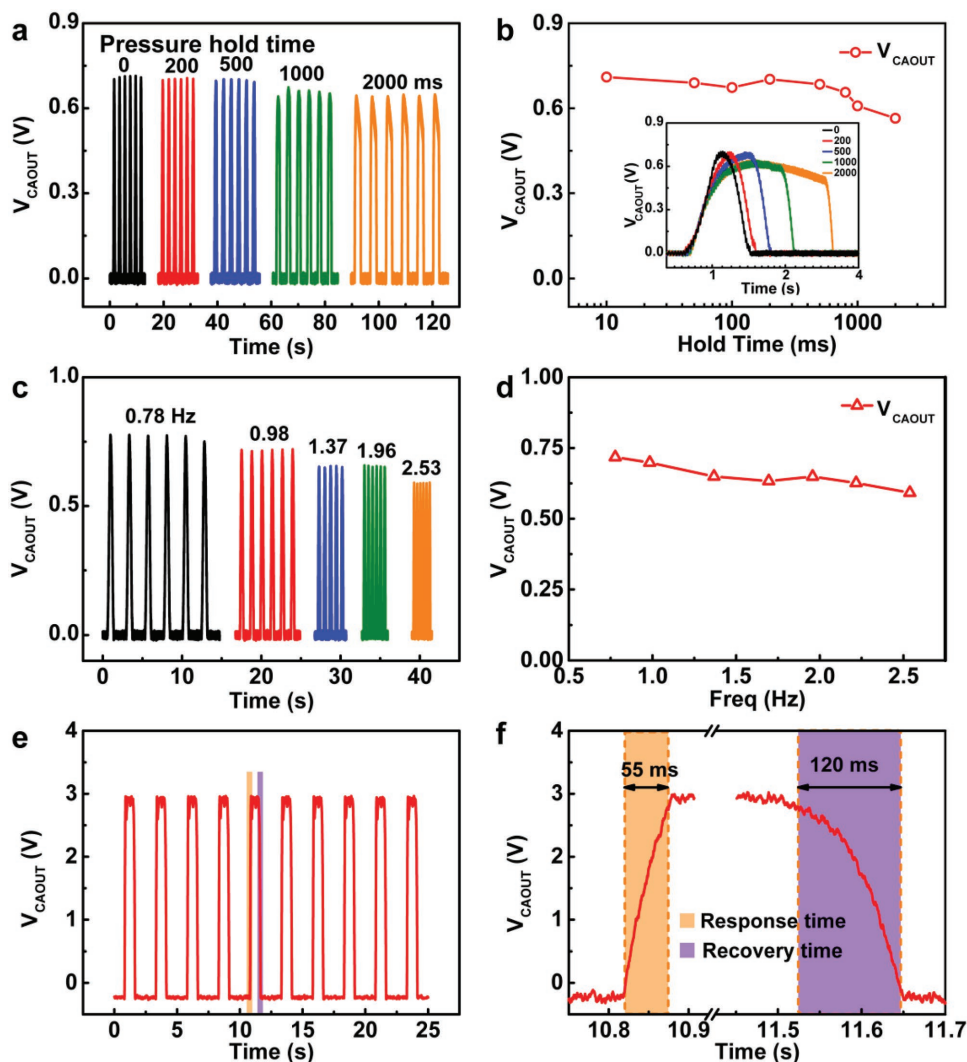
**ADVANCED
SCIENCE NEWS**
www.advancedsciencenews.com

**ADVANCED
FUNCTIONAL
MATERIALS**
www.afm-journal.de

Figure 3. Dynamic responses of the CAmp. a) The real-time measurement of V_{CAOUT} with pressures same in magnitude and motion speed but different in exertion time, applied on the sensor. b) The summarized relationship between the output signal V_{CAOUT} and the pressure holding time applied on PENG-PS. c) The real-time measurement of V_{CAOUT} with pressures applied on the sensor, which is of the same magnitude and exertion time motion but different motion speed. d) The summarized relationship between the output signal V_{CAOUT} and the pressure motion speed applied on PENG-PS. e) Voltage response to a pressure pulse hitting by hammer. f) Time response of the voltage V_{CAOUT} change as the force changes between 10.75 and 11.7 s.

It is noticed that, in period press–hold–release motion, the V_{CAOUT} is influenced by not only the magnitude of the applied pressure, but also the pressure hold time and the motion frequency. As shown in **Figure 3**a,b, it can be observed that the V_{CAOUT} decreased slowly with the rising holding time from 0 to 2000 ms. The applied force was fixed at 16 N, with a motion speed of 100 µm s^{-1}. One of the possible reasons is that charges stored in the capacitor could dissipate through the parallel resistor, so that the V_{CAOUT} drops with the rising pressure hold time. The frequency response shown in Figure S2b in the Supporting Information can also explain it. Figure 3c,d shows the responses of V_{CAOUT} under the same external applied force 15 ± 0.5 N and duration time 10 ms but different frequencies ranging from 0.78 (lowest human gait frequency) to 2.53 Hz (running frequency). It is found that V_{CAOUT} decreased with the frequency's increase. A possible reason is reported in the literature, that the piezoelectric coefficient d_{33} of PVDF or

other piezoelectric materials are frequency-dependent could have contributed to the affected charge amplifier output.[7a] The response time test was also conducted by hitting the sample with a hammer, resulting in a pressure load up to 380 kPa and the amplifier output voltage about 3 V as shown in Figure 3e. We can see from the partial enlarged view (Figure 3f), the response time 55 ms is far less than the biological stance phase (600 ms) and swing-phase (400 ms) and close to the response time of reported tactile sensor.[3e] It demonstrates that the PENG-PS and designed circuit could be applied to monitor foot planar pressure changing during walking.

2.3. Durability of PENG Pressure Sensors and CAmp

As the linearity and dynamic response characteristic, high endurance is also a critical performance for practical applications.
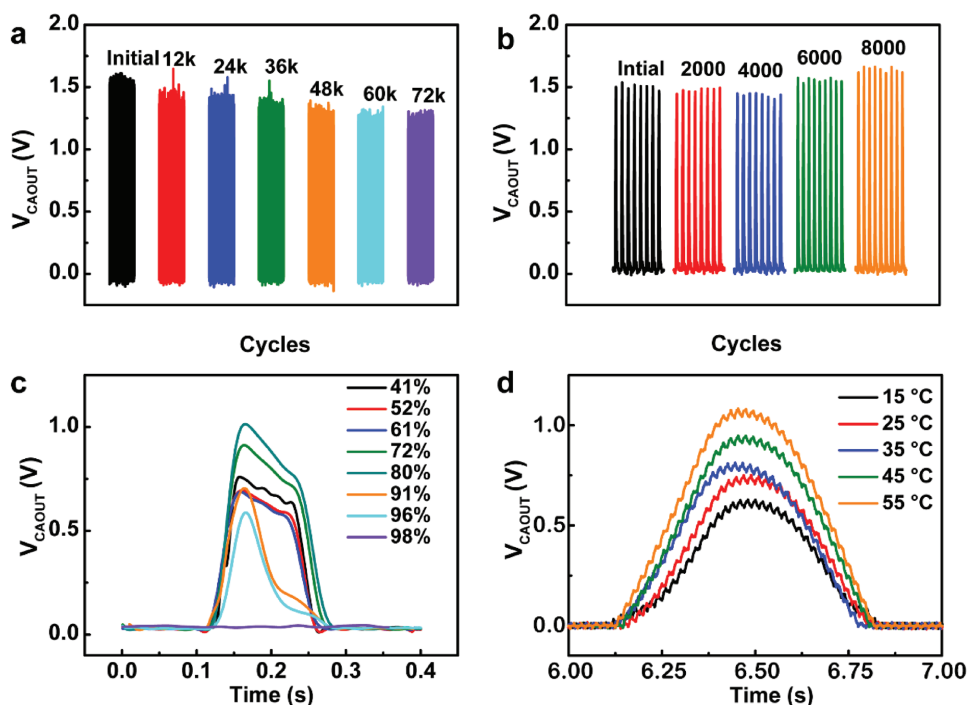
Figure 4. The durability of the PENG-PS and CAmp. a) The stability test PENG-PS and CAmp with continuous loading and unloading a cyclic pressure for over 70 000 cycles, at a frequency of 3.3 Hz. b) The stretch endurance test for pressure sensing of the active sensor with the PVDF-attached FPC continuously bent and released for 80 000 cycles. c) The measurement of the V_{CAOUT} with variable RH levels under 22.5 N. d) The measurement of the V_{CAOUT} with variable temperature under 22.5 N.

Here the endurance tests of a single PENG-PS and whole insole-shaped FPC are shown in **Figure 4**a,b, respectively. The endurance test of single piece was carried out through continuously loading and unloading a constant pressure of 38 N at fixed frequency of 3.3 Hz for over 72 000 cycles. The V_{CAOUT} response was continuously measured and recorded, during which every 12 000 cycles were exhibited in Figure 4a, showing a decay of ≈5.3% after 36 000 cycles and a decay of ≈17% after 72 000 ongoing cycles over a long time span 7.5 h. These decreasing signals might be contributed to the stress introduced by the load and deformation of epoxy. Moreover, the stretch endurance of the whole PVDF-attached FPC performance was also observed in dynamic bending experiments using a PVDF slice sample attached FPC over 8000 cycles. As shown in Figure 4b, the voltage response was measured and displayed by vertical load–unload force of 38 N after every 1000 bending cycles. The charge amplifier output V_{CAOUT} shows a minor float before 6000 stretch–release cycles, and after that, an obvious increase of ≈9.2% could be observed. The possible reason is that the sealed PVDF film was exposed to a periodical and long-time stretching stress, then transforming the α-phase of PVDF into the β-phase.[12] Therefore, a marginal increase in the relative fraction of β-phase was produced, and the higher output was observed. The operation environment, such as moisture atmosphere and various temperature, should be taken into consideration in practical applications, either. The PVDF-attached FPC with matched charge amplifier of which the feedback network contained a 470 pF capacitor and a 6 GΩ resistor was measured under period press–release motion at various humidity or temperature, as shown in Figure 4c,d, respectively. The

response of the PENG-PS was tested at several levels from 40% to 100% relative humidity around 26 ± 2 °C. For the reason that PVDF itself has the characteristic of excellent stability, the main cause of the drastic changes with environment is the gradually reducing circuit stability, especially the resistance between pins of the operator amplifier chip decreasing in the extremely wet condition. As shown in Figure 4c, when the sample is working below 61% rh, the whole system is still reliable, and V_{CAOUT} is float around 0.7 V with the same slope during the constant pressure. In contrast, in the extremely wet condition, the water vapor condenses into droplets and adheres to the surface of electrodes on the DAQ circuit broad, which means decreasing circuit stability and even short-circuit. Therefore, once the relative humidity exceeds 72% rh, the ever-reduced resistance in the feedback loop leads V_{CAOUT} increasing first, then rapidly decreasing to zero with raising leakage current. Therefore both the FPC and the designed circuit should be well packaged to avert the dust or moisture atmosphere. The sensor output was also tested at different temperatures from 15 to 55 °C. As can be seen from Figure 4d, the output voltage of whole system is a strong function of temperature, which is consistent with the reported PVDF-film sensor. This can be solved by software temperature correction or adding a temperature compensation circuit.

2.4. Application as a Smart Insole

To fulfill the potential in pressure monitoring applications, the 32 PENG-PSs are all fixed and connected on the pads of
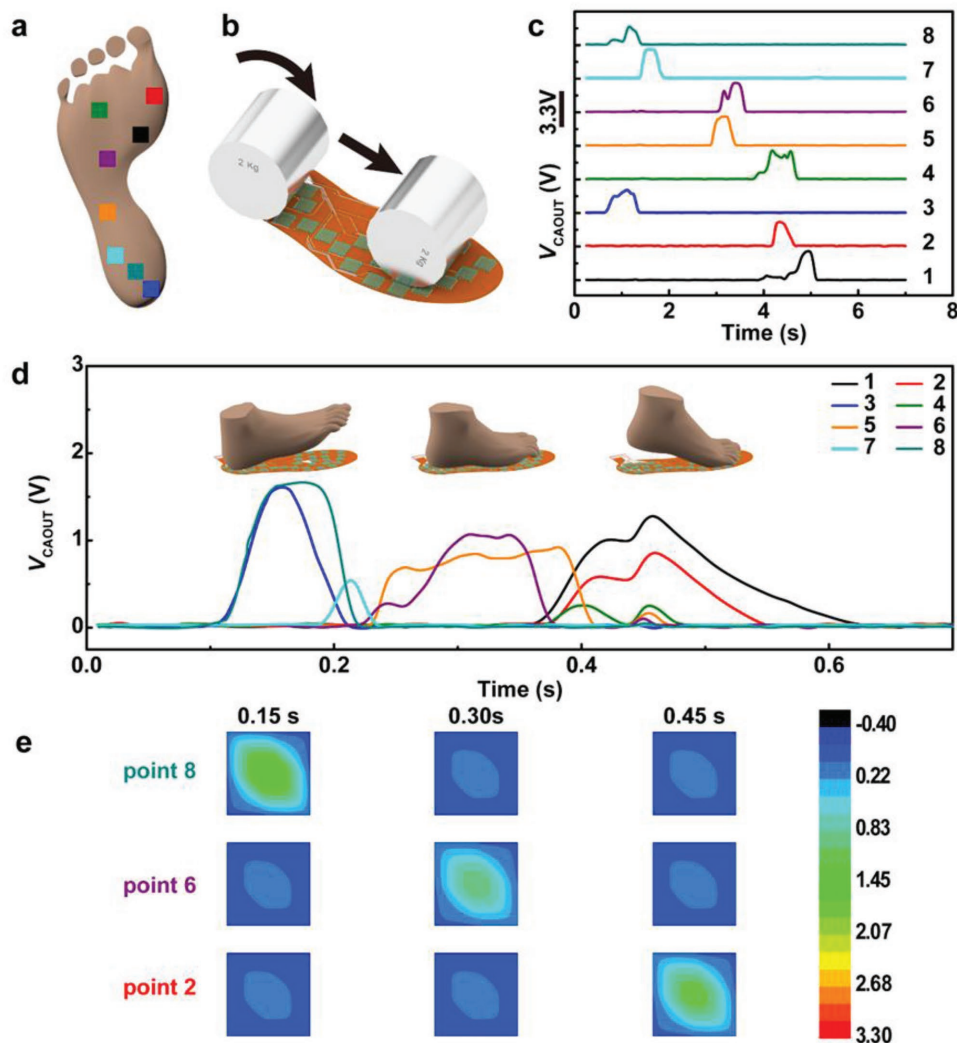
**ADVANCED
SCIENCE NEWS**
www.advancedsciencenews.com

**ADVANCED
FUNCTIONAL
MATERIALS**
www.afm-journal.de

Figure 5. Smart insole based on the fabricated pressure piezo-array. a) Schematic diagram of the placement of selected eight sensor nodes. b) Schematic of a cylinder rolling along different piezo-pixels. c) The real-time measurement of the selected eight sensor nodes in the moving trajectory of the cylinder. e) 2D intensity map reconstructed from d) the real-time measurement of the selected eight sensor nodes under walking motion, the inset parts illustrate the different gait phase.

a sole-shaped FPC, enabling to reflect the pressure distribution, dynamic motion, and mapping in real time. Although more sensor nodes can be easily added on the FPC, a reduced number of sensing points is beneficial to decrease the electron components and area of the circuit broad. We first monitored and recorded the trajectory of moving object to demonstrate the intriguing features of this smart insole. As shown in **Figure 5**a, eight channels on the sensing film were selected to display the tested result. When a 2 kg weight metal cylinder rolled across the insole (Figure 5b), the pressure changed, and the trajectory profile could be clearly recorded in real-time. Apparently, the motion path of weight, moving from heel (the blue, dark cyan, and cyan marks demonstration in Figure 5a), to the lateral (the orange one), till the forefoot (the black, red, and green squares), was distinguished in the graph, which was very similar to the voltage signal change of nodes depicted in Figure 5c. Notably, the diversities of waveform observed in the V_{CAOUT} response is due to that the FR4 thin slices for encapsulation could block

the rolling. The change of dynamic charge and corresponding output voltage can be monitored in real time through the sensors. As shown in Figure 5d, the three insets are the schematics of heel striking, standing phase, and pushing off through toes, respectively. The responses at the sensors of point 3 (the blue line) and point 7 (the dark cyan line) are clearly in front of the others, since the heel touches the ground first under walking station. According to the measured voltage signals, reconstructed intensity map of three independent sensor nodes numbered 2, 6, and 8 (the red, purple, and dark cyan lines in panel (d) and squares with the same color in panel (a)) are plotted by Origin software to fill a diametric, in which the color represents the different magnitude of V_{CAOUT}, as shown in Figure 5e at 0.15, 0.30, and 0.45 s. It is obvious that these pseudo color maps could demonstrate the magnitude of pressure over time.

To monitor and visually display the foot pressure at real time, the whole self-designed DAQ broad was developed, which was integrated with 32 signals conditioning (charge amplifier)
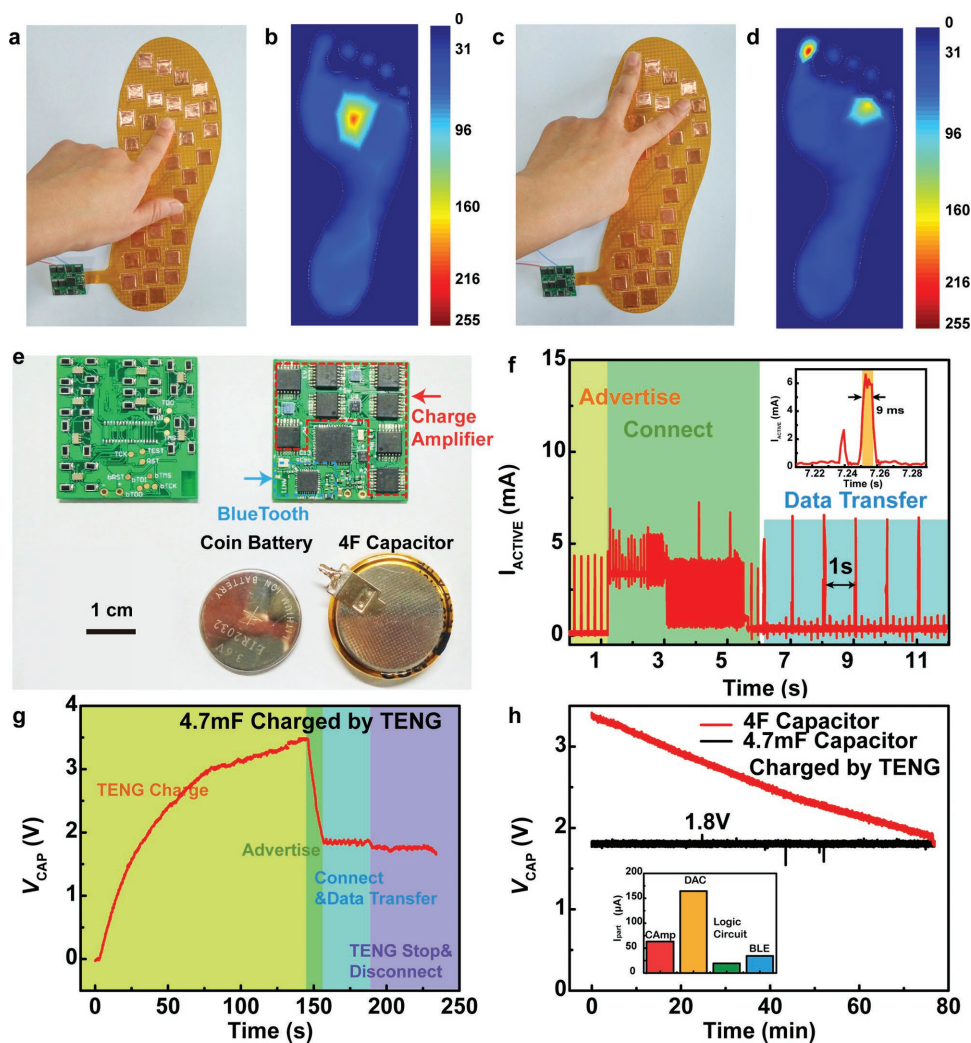
Figure 6. Demonstration of smart insole for plantar pressure mapping system. a) Photograph of the foot pressure mapping system one-point contact. b) A screenshot image of pressure distribution reconstructing performed on the application software developed in Android in the motion of inset (a). c) Photograph of the foot pressure mapping system two-point contact. d) Corresponding reconstructed results in inset (c) performed on the application software. e) Optical photograph of DAQ PCB broad and 4 F capacitor and a coin battery. f) The working current changes with timing sequence of DAQ, which includes advertising period, connecting period, and data transferring period, which are highlighted by yellow, green, and blue respectively. The inset demonstrates the peak current during the data transferring period. g) The real-time measurement of charging and discharging curve of 4 mF charged by a hybridized nanogenerator to drive the DAQ. h) Using a 4 mF capacitor charged by the hybridized nanogenerator or a 4 F capacitor to drive the DAQ. The inset parts demonstrate the current consumption of each parts in DAQ.

channels, a mix-signal microcontroller, and a Bluetooth module. As shown in **Figure 6**a,c, under the circumstances of one point contact and two-point contact by barely finger(s), the pressure distribution can be reconstructed as pseudo color intensity map on a self-developed android application software. The screenshot images are demonstrated in the Figure 6b,d, respectively. It is obvious that when pressed by two fingers, an evident voltage rise of nodes could be seen, but others kept the same V_{CAOUT} and intensity-associated color. In this test, a continuous image of foot plantar pressure can be reconstructed and refreshed in real time from the data transferred by the DAQ broad with 8-bit analog–digital conversion accuracy and typical error of ± 3.5 least significant bit (LSB), meaning only ± 0.045 V error induced by analog to digital converter (ADC) operation. A short video of demonstrating the sensing and reconstructing

process is provided in Video S1 in the Supporting Information. In this video, a 100 pF feedback capacitor was utilized to obtain a sensitive and prominent visual pressure distribution image.

2.5. Integrating with a Hybridized Triboelectric–Electromagnetic Nanogenerator as a Self-Powered System

Considering the requirement of portable applications, the DAQ is a compact and low power–consumption design with both Bluetooth module and analog processing circuit all integrated in a single board with the size of 27.5×27.5 mm^2, similar to the size of a button battery in Figure 6e. As depicted in Figure S3 in the Supporting Information, the foot pressure signals acquired by the FPC with PENG-PS would be processed in the DAQ circuit

**ADVANCED
SCIENCE NEWS**
www.advancedsciencenews.com

**ADVANCED
FUNCTIONAL
MATERIALS**
www.afm-journal.de

broad, which includes the charge amplifiers, analog switches, mixed-signal microcontroller (MS-MCU), and Bluetooth module. The 32 channels analog signals are divided into two groups by 16 double-pole-double-throw (DPDT) complementary metal-oxide-semiconductor (CMOS) analog switches under the control of MS-MCU. Then these analog foot pressure signals are converted into a digital signal the ADC module embedded in the MS-MCU in order of channels. The converted digital signal is send to smart phone through Bluetooth module. The Figure 6f demonstrated that the working current varied with the switching between different working situations, including advertising period, connecting period, and data transferring period, highlighted by yellow, green, and blue, respectively. During the advertising period, the DAQ circuit is in low-power-mode with a quiescent current lower than 100 μA to ensure that the integrated Bluetooth module will not stop advertising with a peak current consumption of 4.5 mA. When a client device, such as pad, laptop, and smart phone, issues a connecting request, it will trigger the DAQ circuit waking up and starting processing the signals acquiring. After the connection, the DAQ works in data transferring period. During this period, the data converted from 32 analog channels would be transferred through Bluetooth Low Energy (BLE) in air in 1 s, producing an average current consumption of 260 μA and a 9 ms durating peak current up to 6.7 mA, as shown in the insets of Figure 6f. In total, the average consumption current is 260 μA, when the operation voltage is 1.8 V, and thus, the mean power of the circuit is 0.47 mW. Meanwhile, as a cost-effective and environmentally friendly technology to converting low-frequency mechanical energies into electricity or sensing mechanical agitations, the TENG is capable of harvesting biomechanical energy from daily motion like walking,[11a–c] and mechanical energy in ambient environment, like rain and water wave.[14] The TENG has reached to 500 W m^{-2},[15] and been used to capture particulate matter (PMs),[16] manipulating the movement of both microfluid and solid objects,[17] and driven wearable electronics and sensors. In this paper, the DAQ could be combined with a hybridized triboelectric–electromagnetic nanogenerator,[11a] developing a continuous and self-powered pressure mapping system, as illustrated in Figure 6g. The charging–discharging curve of the capacitor V_{CAP} also demonstrates the timing-sequence. The voltage of capacitor can reach 3.5 V charged by hybridized nanogenerator before connected to the DAQ circuit, and then dropped rapidly for the advertising and connecting processing. After that, the DAQ went into the data-transferring operation condition continuously, with the circuit voltage of 1.8 V, driven by the hybridized nanogenerator. When the nanogenerator was disconnected, the voltage dropped and the DAQ stopped working, as illustrated in Figure 6g. Moreover, a precharged 4F capacitor can maintain 76 min uninterrupted data transferring after the nanogenerator was disconnected. Current consumptions of each parts in DAQ, including 32 CAmps, ADC, logic circuit, and BLE 4.2 protocol module are measured and displayed in the inset part in Figure 6h.

3. Conclusion

In summary, a self-powered smart insole plantar pressure mapping system was presented based on piezoelectric, triboelectirc,

and electromagnetic Nanogenerators. The PVDF-based PENG pressure sensor and the employed charge amplifier exhibited fast response, good linearity relationship with external force. The measurement span was wide up to 200 kPa, and the durability was demonstrated, including 200 kPa pressure load and 8000 bending–releasing cycles. More attractively, a designed signal acquisition circuit integrated with Bluetooth technology could wirelessly transmit the pressure signals onto a smart phone for real-time foot pressure monitoring. And the whole system can work continuously, under driven by a hybridized triboelectric–electromagnetic nanogenerator, achieving a self-powered insole monitoring system. This work will enlighten smart applications in footwear design, sport/exercise biomechanics information acquisition, injury prevention, as well as diabetes ulceration prediction.

Conflict of Interest

The authors declare no conflict of interest.

[1] a) H. Ouyang, J. Tian, G. Sun, Y. Zou, Z. Liu, H. Li, L. Zhao, B. Shi, Y. Fan, Y. Fan, Z. L. Wang, Z. Li, *Adv. Mater.* **2017**, *29*, 1703456; b) W. Tang, J. Tian, Q. Zheng, L. Yan, J. Wang, Z. Li, Z. L. Wang, *ACS Nano* **2015**, *9*, 7867; c) Q. Zheng, B. Shi, F. Fan, X. Wang, L. Yan, W. Yuan, S. Wang, H. Liu, Z. Li, Z. L. Wang, *Adv. Mater.* **2014**, *26*, 5851.

[2] a) M. Liu, X. Pu, C. Jiang, T. Liu, X. Huang, L. Chen, C. Du, J. Sun, W. Hu, Z. L. Wang, *Adv. Mater.* **2017**, *29*, 1703700; b) W. Song, B. Gan, T. Jiang, Y. Zhang, A. Yu, H. Yuan, N. Chen, C. Sun, Z. L. Wang, *ACS Nano* **2016**, *10*, 8097; c) S. Lee, R. Hinchet, Y. Lee, Y. Yang, Z. H. Lin, G. Ardila, L. Montes, M. Mouis, Z. L. Wang, *Adv. Funct. Mater.* **2014**, *24*, 1163.

[3] a) Q. Hua, J. Sun, H. Liu, R. Bao, R. Yu, J. Zhai, C. Pan, Z. L. Wang, *Nat. Commun.* **2018**, *9*, 244; b) X. X. Zhu, X. S. Meng, S. Y. Kuang, X. D. Wang, C. F. Pan, G. Zhu, Z. L. Wang, *Nano Energy* **2017**, *41*, 387; c) U. Khan, T. H. Kim, H. Ryu, W. Seung, S. W. Kim, *Adv. Mater.* **2017**, *29*, 1603544; d) W. Li, D. Torres, R. Diaz, Z. Wang, C. Wu, C. Wang, Z. Lin Wang, N. Sepulveda, *Nat. Commun.* **2017**, *8*, 15310; e) Z. W. Yang, Y. Pang, L. Zhang, C. Lu, J. Chen, T. Zhou, C. Zhang, Z. L. Wang, *ACS Nano* **2016**, *10*, 10912; f) J. Luo, W. Tang, F. R. Fan, C. Liu, Y. Pang, G. Cao, Z. L. Wang, *ACS Nano* **2016**, *10*, 8078; g) J. Yang, J. Chen, Y. Su, Q. Jing, Z. Li, F. Yi, X. Wen, Z. Wang, Z. L. Wang, *Adv. Mater.* **2015**, *27*, 1316; h) J. Luo, F. R. Fan, T. Zhou, W. Tang, F. Xue, Z. L. Wang, *Extreme Mech. Lett.* **2015**, *2*, 28; i) W. Tang, T. Zhou, C. Zhang, F. R. Fan, C. B. Han, Z. L. Wang, *Nanotechnology* **2014**, *25*, 225402; j) L. Lin, Y. Xie, S. Wang, W. Wu, S. Niu, X. Wen, Z. L. Wang, *ACS Nano* **2013**, *7*, 8266; k) G. Zhu, C. Pan, W. Guo, C. Y. Chen, Y. Zhou, R. Yu, Z. L. Wang, *Nano Lett.* **2012**, *12*, 4960.

[4] Z. Lin, J. Chen, X. Li, Z. Zhou, K. Meng, W. Wei, J. Yang, Z. L. Wang, *ACS Nano* **2017**, *11*, 8830.

[5] Q. Zhang, Q. Liang, Z. Zhang, Z. Kang, Q. Liao, Y. Ding, M. Ma, F. Gao, X. Zhao, Y. Zhang, *Adv. Funct. Mater.* **2018**, *28*, 1703801.

[6] a) K. Y. Lee, H.-J. Yoon, T. Jiang, X. Wen, W. Seung, S.-W. Kim, Z. L. Wang, *Adv. Energy Mater.* **2016**, *6*, 1502566; b) S. Chen, B. Zhuo, X. Guo, *ACS Appl. Mater. Interfaces* **2016**, *8*, 20364; c) X. Qiu, D. H. Tian, C. L. Han, W. Chen, Z. J. Wang, Z. Y. Mu, K. Z. Liu, *China Med. J.* **2015**, *128*, 3283; d) A. H. A. Razak, A. Zayegh, R. K. Begg, Y. Wahab, *Sensors* **2012**, *12*, 9884; e) J. A. Ramirez-Bautista, J. A. Huerta-Ruelas, S. L. Chaparro-Cardenas, A. Hernandez-Zavala, *IEEE Rev. Biomed. Eng.* **2017**, *10*, 299.

[7] a) S. Liu, L. Wang, X. Feng, Z. Wang, Q. Xu, S. Bai, Y. Qin, Z. L. Wang, *Adv. Mater.* **2017**, *29*, 1606346; b) L. Wang, S. Liu, X. Feng, Q. Xu, S. Bai, L. Zhu, L. Chen, Y. Qin, Z. L. Wang, *ACS Nano* **2017**, *11*, 4859; c) F. R. Fan, W. Tang, Z. L. Wang, *Adv. Mater.* **2016**, *28*, 4283; d) W. Wu, X. Wen, Z. L. Wang, *Science* **2013**, *340*, 952; e) Z. L. Wang, *Chin. Sci. Bull.* **2009**, *54*, 4021.

[8] S. Xu, B. J. Hansen, Z. L. Wang, *Nat. Commun.* **2010**, *1*, 93.

[9] W. Z. Wu, L. Wang, Y. L. Li, F. Zhang, L. Lin, S. M. Niu, D. Chenet, X. Zhang, Y. F. Hao, T. F. Heinz, J. Hone, Z. L. Wang, *Nature* **2014**, *514*, 470.

[10] a) S. Wang, Z. L. Wang, Y. Yang, *Adv. Mater.* **2016**, *28*, 2881; b) V. Bhavanasi, V. Kumar, K. Parida, J. Wang, P. S. Lee, *ACS Appl. Mater. Interfaces* **2016**, *8*, 521; c) X. Wang, B. Yang, J. Liu, Y. Zhu, C. Yang, Q. He, *Sci. Rep.* **2016**, *6*, 36409; d) Y. Mao, P. Zhao, G. McConohy, H. Yang, Y. Tong, X. Wang, *Adv. Energy Mater.* **2014**, *4*, 1301624; e) C. Chang, V. H. Tran, J. Wang, Y. K. Fuh, L. Lin, *Nano Lett.* **2010**, *10*, 726; f) A. V. Shirinov, W. K. Schomburg, *Sens. Actuators, A* **2008**, *142*, 48.

[11] a) L. Liu, W. Tang, C. Deng, B. Chen, K. Han, W. Zhong, Z. L. Wang, *Nano Res.* **2018**, https://doi.org/10.1007/s12274-018-1978-z; b) J. Wang, S. Li, F. Yi, Y. Zi, J. Lin, X. Wang, Y. Xu, Z. L. Wang, *Nat. Commun.* **2016**, *7*, 12744; c) J. Luo, F. R. Fan, T. Jiang, Z. Wang, W. Tang, C. Zhang, M. Liu, G. Cao, Z. L. Wang, *Nano Res.* **2015**, *8*, 3934; d) K. Zhang, X. Wang, Y. Yang, Z. L. Wang, *ACS Nano* **2015**, *9*, 3521; e) J. Y. Youfan Hu, S. Niu, W. Wu, Z. L. Wang, *ACS Nano* **2014**, *8*, 7442; f) C. Zhang, W. Tang, C. Han, F. Fan, Z. L. Wan, *Adv. Mater.* **2014**, *26*, 3580.

[12] V. Sencadas, R. G. Jr., S. Lanceros-Méndez, *J. Macromol. Sci., Part B: Phys.* **2009**, *48*, 514.

[13] a) Z. L. Wang, *Mater. Today* **2017**, *20*, 74; b) L. Persano, C. Dagdeviren, Y. Su, Y. Zhang, S. Girardo, D. Pisignano, Y. Huang, J. A. Rogers, *Nat. Commun.* **2013**, *4*, 1633.

[14] a) L. M. Zhang, C. B. Han, T. Jiang, T. Zhou, X. H. Li, C. Zhang, Z. L. Wang, *Nano Energy* **2016**, *22*, 87; b) Q. J. Liang, X. Q. Yan, Y. S. Gu, K. Zhang, M. Y. Liang, S. N. Lu, X. Zheng, Y. Zhang, *Sci. Rep.* **2015**, *5*, 9080; c) T. X. Xiao, T. Jiang, J. X. Zhu, X. Liang, L. Xu, J. J. Shao, C. L. Zhang, J. Wang, Z. L. Wang, *ACS Appl. Mater. Interfaces* **2018**, *10*, 3616.

[15] a) F. Xi, Y. Pang, W. Li, T. Jiang, L. Zhang, T. Guo, G. Liu, C. Zhang, Z. L. Wang, *Nano Energy* **2017**, *37*, 168; b) Y. Zi, H. Guo, J. Wang, Z. Wen, S. Li, C. Hu, Z. L. Wang, *Nano Energy* **2017**, *31*, 302; c) L. Li, *Sci. Bull.* **2015**, *60*, 1626; d) G. Zhu, Y. S. Zhou, P. Bai, X. S. Meng, Q. Jing, J. Chen, Z. L. Wang, *Adv. Mater.* **2014**, *26*, 3788; e) F.-R. Fan, Z.-Q. Tian, Z. Lin Wang, *Nano Energy* **2012**, *1*, 328.

[16] a) C. B. Han, T. Jiang, C. Zhang, X. Li, C. Zhang, X. Cao, Z. L. Wang, *ACS Nano* **2015**, *9*, 12552; b) Y. Bai, C. B. Han, C. He, G. Q. Gu, J. H. Nie, J. J. Shao, T. X. Xiao, C. R. Deng, Z. L. Wang, *Adv. Funct. Mater.* **2018**, *28*, 1706680.

[17] a) L. Zheng, Y. Wu, X. Chen, A. Yu, L. Xu, Y. Liu, H. Li, Z. L. Wang, *Adv. Funct. Mater.* **2017**, *27*, 1606408; b) J. Nie, Z. Ren, J. Shao, C. Deng, L. Xu, X. Chen, M. Li, Z. L. Wang, *ACS Nano* **2018**, *12*, 1491.

1801606 (9 of 9)